New Journal of Physics
The open-access journal for physics

Collective orbital excitations in orbitally ordered YVO_3 and $HoVO_3$

E Benckiser[1], R Rückamp[2], T Möller[1], T Taetz[3], A Möller[3], A A Nugroho[4,5], T T M Palstra[5], G S Uhrig[6] and M Grüninger[1,7]

[1] II. Physikalisches Institut, Universität zu Köln, Zülpicher Strasse 77, 50937 Köln, Germany
[2] 2. Physikalisches Institut A, RWTH Aachen University, 52056 Aachen, Germany
[3] Institut für Anorganische Chemie, Universität zu Köln, 50939 Köln, Germany
[4] Jurusan Fisika, Institut Teknologi Bandung, Jl. Ganesha 10, Bandung 40132, Indonesia
[5] Zernike Institute for Advanced Materials, University of Groningen, Nijenborgh 4, 9747 AG Groningen, The Netherlands
[6] Theoretische Physik I, Technische Universität Dortmund, 44221 Dortmund, Germany
E-mail: grueninger@ph2.uni-koeln.de

New Journal of Physics **10** (2008) 053027 (21pp)
Received 20 March 2008
Published 20 May 2008
Online at http://www.njp.org/
doi:10.1088/1367-2630/10/5/053027

Abstract. We study orbital excitations in the optical absorption spectra of YVO_3 and $HoVO_3$. We focus on an orbital absorption band observed at 0.4 eV for polarization $E \parallel c$. This feature is only observed in the intermediate, monoclinic phase. By comparison with the local crystal-field (CF) excitations in VOCl and with recent theoretical predictions for the CF levels we show that this absorption band cannot be interpreted in terms of a local CF excitation. We discuss a microscopic model which attributes this absorption band to the exchange of two orbitals on adjacent sites, i.e. to the direct excitation of two orbitons. This model is strongly supported by the observed dependence on polarization and temperature. Moreover, the calculated spectral weight is in good agreement with the experimental result.

[7] Author to whom any correspondence should be addressed.

Contents

1. Introduction

In strongly correlated transition-metal oxides, orbital interactions play a key role in many intriguing phenomena such as the colossal magnetoresistance or the effective reduction of dimensionality [1]–[4]. Orbitals on different sites interact with each other [5, 6] via the collective Jahn–Teller effect, i.e. the coupling to the lattice, and via exchange interactions, which are governed by the antisymmetrization of the total wavefunction including both the orbital and the spin part. These interactions can result in coupled long-range spin and orbital order. If the coupling to the lattice is dominant, the excitations are well described by 'local' crystal-field (CF) excitations [7]–[9], where 'local' means that the excitation can be treated as a change of the orbital occupation on a *single* site, i.e. the dispersion is negligible. In the opposite case of dominant exchange interactions, one expects novel collective elementary excitations, namely orbital waves (orbitons) with a significant dispersion [10], reflecting the propagation of the excited state. Thus orbitons are analogous to spin waves—propagating spin flips—in a magnetically ordered state. Orbitons are expected to reveal the fundamental orbital interactions responsible for the interesting physical properties. In the quest for the experimental observation of orbitons, the central experimental task is to demonstrate that the orbital exchange interactions are essential for the elementary excitations. If this is the case, the excitations cannot be described in terms of single-site physics, and we will use the term 'orbiton'.

The first claim for the observation of orbitons was based on Raman data of $LaMnO_3$ [11], but the relevant features have later been explained in terms of multi-phonons [12]. In fact, in the manganites the orbital degree of freedom is connected with e_g electrons, for which the coupling to the lattice is strong in an octahedral environment. The vanadates RVO_3 with two electrons occupying t_{2g} orbitals may be considered as more promising candidates [13]–[15]. Recently, the observation of orbitons in Raman data of RVO_3 ($R = $ Y, La, Nd) has been claimed at 43 and 62 meV by Miyasaka *et al* [16, 17] and at 45 and 84 meV by Sugai and Hirota [18], but the proposed orbitons are hard to discriminate from (multi-)phonons and magnons, and the assignment is controversial [16]–[18]. In $YTiO_3$ and $LaTiO_3$, a Raman peak at 0.25 eV has been interpreted in terms of a two-orbiton excitation, based on its dependence on temperature, polarization, and on the frequency of the incoming photons [19, 20]. However, it cannot be fully excluded that this feature corresponds to a local CF excitation [9]. Thus, an experimental proof for the existence of orbitons is still lacking.

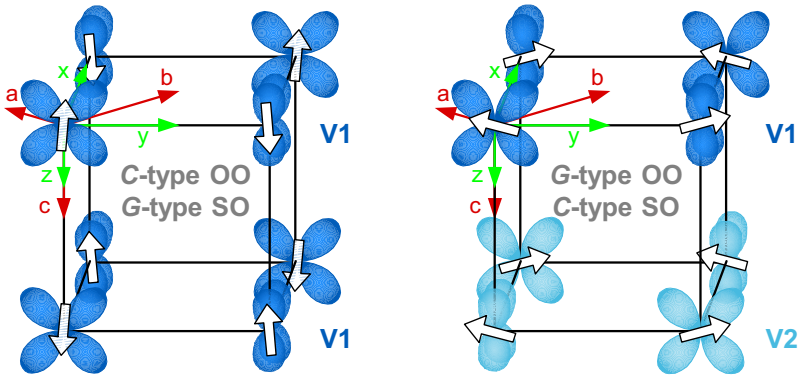

(a) $T < 77$ K (*Pbnm*) (b) 77 K $< T <$ 200 K ($P2_1/b$)

Figure 1. Orbital and spin ordering patterns in YVO_3 for (a) $T_S < 77$ K and (b) $T_S < T < T_{OO} = 200$ K [15], [21]–[32]. The xy orbital is occupied by one electron on each site (not shown). The occupation of xz and yz orbitals is C-type below T_S and G-type above (see main text for more details). SO is lost at $T_N = 116$ K. The coordinates of the *Pbnm* and $P2_1/b$ crystal systems are given in the upper left corner of each figure.

Here, we report on the observation of orbital excitations in the optical conductivity $\sigma(\omega)$ of orbitally ordered YVO_3 and $HoVO_3$. We focus on an absorption feature observed for $E \parallel c$ at about 0.4 eV, well above the range of phonons and magnons and well below the Mott–Hubbard gap. A comparison with the local CF excitations in the $3d^2$ system VOCl and with recent theoretical results [15, 21] for the CF levels shows that this feature is hard to reconcile with a local CF scenario, in particular, as far as the energy, the polarization and temperature dependence are concerned. We discuss the microscopic exchange process and conclude that the feature at 0.4 eV reflects the exchange of two orbitals on neighboring sites, i.e. the direct excitation of two orbitons.

The vanadates RVO_3 with $R =$ Y and Ho exhibit an orthorhombic crystal structure (*Pbnm*) at room temperature [22, 23, 33]. The undoped compounds represent Mott–Hubbard insulators with two localized electrons in the $3d$ shell of each V^{3+} ion. A crystal field of predominantly octahedral symmetry yields a splitting of the $3d$ states into a lower-lying, triply degenerate t_{2g} level and a doubly degenerate e_g level. A detailed analysis of the structure reveals that the degeneracy of these levels is fully lifted by an orthorhombic distortion of the VO_6 octahedra (D_{2h} symmetry) [22, 23], giving rise to a splitting of the t_{2g} manifold into xy, xz and yz orbitals. In YVO_3, a low-temperature orthorhombic phase (*Pbnm*) with G-type spin order (SO) and C-type orbital order (OO) was found below $T_S = 77$ K [15], [21]–[32], i.e. the xy orbital is occupied at each V site, whereas the occupation of xz and yz orbitals alternates within the ab-plane (see figure 1). At $T_S = 77$ K, a first-order structural phase transition to an intermediate, monoclinic phase with $P2_1/b$ symmetry has been observed. This monoclinic phase shows two different vanadium sites, V(1) and V(2), which alternate along the c-axis. Therefore, the mirror symmetry perpendicular to the ab-plane is broken in the intermediate phase. The spin ordering pattern changes from G-type below T_S to C-type above. Long-range magnetic order is lost at $T_N = 116$ K. The structural phase transition from the monoclinic phase to the orthorhombic room-temperature phase is observed at $T_{OO} \approx 200$ K, which has been interpreted

as the long-range orbital ordering temperature [22]. However, synchrotron x-ray diffraction data give evidence for the presence of OO up to about 300 K [28]. For the intermediate monoclinic phase, it has been discussed controversially whether the physics has to be described in terms of 'classical' OO or quantum orbital fluctuations: it has been proposed that the intermediate phase of YVO_3 represents the first realization of a one-dimensional orbital liquid and of an orbital Peierls phase with V(1)–V(2) orbital dimers [14], [34]–[37]. This has been challenged by LDA+U and LDA+DMFT studies [15, 31], which for YVO_3 find OO and that at least below 300 K orbital quantum fluctuations are suppressed in YVO_3 by a sizeable ligand-field splitting. The orbital ordering pattern in the monoclinic phase has been reported as G-type based on, e.g. resonant x-ray diffraction [28], an analysis of the V–O bond lengths [24], or LDA+U calculations [31]. In comparison to C-type OO, the orbitals of every second layer along c are shifted along x, thus xz and yz alternate along x, y and z for G-type OO (see figure 1). According to Hartree–Fock calculations, the size of $GdFeO_3$-type distortions is decisive for the choice between G-type and C-type OO patterns [30]. A recent LDA+DMFT study by De Raychaudhury *et al* finds that the OO pattern is intermediate between C-type and G-type due to the $GdFeO_3$ distortions, almost C-type in the intermediate phase [15]. However, Noguchi *et al* [28] claim that their synchrotron x-ray diffraction data are fitted best by G-type OO, but that the partial occupation of other orbitals is possible. The compound $HoVO_3$ behaves very similar to YVO_3 with slightly different phase-transition temperatures of $T_{OO} \approx 188$ K, $T_N = 114$ K and $T_S \approx 40$ K [33, 38]. A detailed structural study of $HoVO_3$ using both neutron and synchrotron x-ray scattering concludes on the basis of the V–O bond lengths that the intermediate monoclinic phase exhibits G-type OO with significant orbital fluctuations, but that these fluctuations are not strong enough to establish an orbitally dimerized state [38].

The paper is organized as follows. In section 2, we address the crystal growth and characterization as well as the optical measurements. The optical conductivity of YVO_3 is discussed in section 3. We first establish the orbital character of the excitations observed between 0.2 and 0.8 eV. In a second step, we argue that the peak observed at 0.4 eV for $E \parallel c$ cannot be interpreted as a local CF excitation. Then, we propose that the observed feature can be understood as a two-orbiton absorption and discuss its energy, polarization and temperature dependence. We derive an effective Hamiltonian for the orbital exchange process and calculate the spectral weight of the considered two-orbiton excitation. In order to corroborate our interpretation, we present data of $HoVO_3$. Finally, we address the peak observed at 0.55 eV for $E \parallel a$. The results are summarized in section 4. The derivation of the effective Hamiltonian is described in the appendix, discussing the remarkable difference between the standard unitary transformation and a continuous unitary transformation.

2. Experiment

Single crystals of RVO_3 with $R =$ Y and Ho have been grown by the traveling-solvent floating-zone method [22]. The purity, stoichiometry and single-phase structure of the crystals were checked by x-ray diffraction and thermogravimetry. Typical crystal dimensions are a few millimeters along all three crystallographic axes. The optical conductivity $\sigma(\omega)$ of YVO_3 was determined by measuring both the transmittance and the reflectance [39] between 0.06 and 1.9 eV using a Fourier spectrometer. The measurements have been performed using linearly polarized light with the electric field parallel to the orthorhombic axes, i.e. $E \parallel a$, b and c

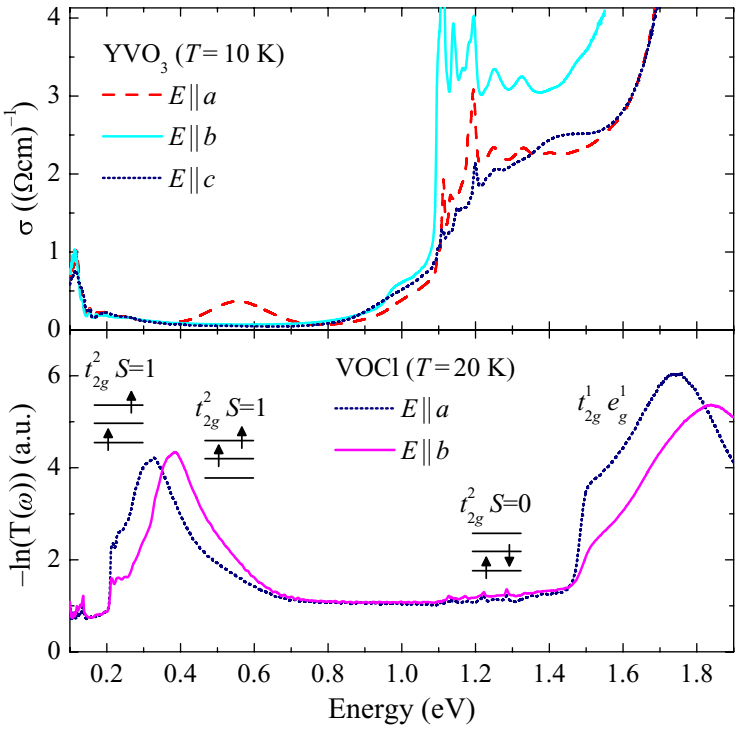

Figure 2. Optical conductivity of YVO_3 in the low-temperature orthorhombic phase at $T = 10\,\mathrm{K}$ for $E \parallel a$, b and c (top panel) and $-\ln(\mathrm{T}(\omega))$ of VOCl at 20 K for $E \parallel a$ and b (in *Pmmn*; bottom panel). Three different orbital excitations within the t_{2g} subshell are sketched in the lower panel.

(see top panel of figure 2). For convenience, we use the same set of axes at all temperatures, i.e. we neglect the monoclinic distortion of the structure. This is justified because the monoclinic angle $\alpha = 89.98^\circ$ is very close to 90° [22]. The reflectance was measured on samples with a thickness of $d > 2\,\mathrm{mm}$ in order to avoid backside reflections. The transmittance data were collected on a series of crystals with different thickness ($100\,\mu\mathrm{m} < d < 500\,\mu\mathrm{m}$), which were polished on both the sides.

Single crystals of VOCl have been grown by the chemical-vapor transport technique. The purity of the crystals was checked by x-ray powder diffraction. Typical crystal dimensions are a few mm^2 in the ab-plane and 10–100 μm along the c-axis. In the case of VOCl and $HoVO_3$, we have measured the transmittance only. The transmittance $\mathrm{T}(\omega)$ is a very sensitive probe for the determination of weakly infrared-active excitations below the gap of these Mott–Hubbard insulators, where the reflectance is nearly constant and featureless. Therefore, the absorption coefficient $\alpha(\omega) \propto -\ln(\mathrm{T}(\omega))/d$ can be used equivalently to $\sigma(\omega)$ for the determination of weak orbital excitations [39].

3. Results and discussion

The top panel of figure 2 shows the optical conductivity $\sigma(\omega)$ of YVO_3 at 10 K in the transparent window of the Mott–Hubbard insulator, i.e. above the phonon range and below the electronic interband excitations. The lowest electronic transition corresponds to an excitation across the Mott–Hubbard gap, i.e. the transfer of one electron from a $3d^2$ V^{3+} site to another one,

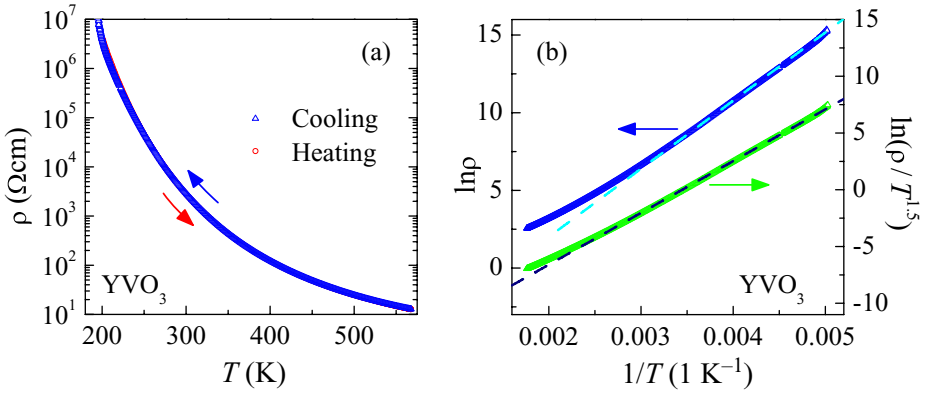

Figure 3. (a) Resistivity ρ of YVO_3 from $T = 200\,\mathrm{K}$ up to 570 K. (b) $\ln(\rho)$ versus $1/T$ (left axis) and $\ln(\rho/T^{3/2})$ versus $1/T$ (right axis). Dashed lines show fits for activated behavior (left axis) and within the non-adiabatic small-polaron model (right).

$3d^2\,3d^2 \rightarrow 3d^1\,3d^3$. In the optical conductivity, the lowest electronic excitation is observed at 1.8 eV [27, 40], and a value of 1.6 eV has been reported for the Mott–Hubbard gap based on a combination of ellipsometry and LSDA + U calculations [27]. This agrees with the steep increase of $\sigma(\omega)$ in our data (see top panel of figure 2). However, the transmittance reveals that the very onset of excitations across the Mott–Hubbard gap is somewhat lower. The precise onset is obscured by the superposition of spin-forbidden orbital excitations between about 1.0 and 1.5 eV (see below). Charge-transfer excitations, involving the transfer of an electron between V and O ions ($d^2 \rightarrow d^3\bar{L}$), are located above about 4 eV [27]. Absorption features below the Mott–Hubbard gap have to be attributed to phonons, magnons, excitons, orbital excitations or to localized carriers trapped by impurities. We exclude the latter for a number of reasons: (i) the spectra of different samples of YVO_3 are identical, (ii) the spectra of YVO_3 and $HoVO_3$ are very similar (see below), (iii) the polarization and temperature dependence (see below), and (iv) the dc resistivity, which is very large, $3 \times 10^6\,\Omega$cm at 200 K. In earlier experiments, an activation energy of $\Delta_{\mathrm{act}} = 0.25$ eV was obtained for polycrystalline samples from resistivity data for $180\,\mathrm{K} < T < 300\,\mathrm{K}$ [41], corresponding to an optical gap of $2\Delta_{\mathrm{act}} = 0.5$ eV. In figure 3(a), we plot $\rho(T)$ of our single crystals between 200 and 570 K. Note that $\rho(T)$ is about an order of magnitude larger than reported in [41]. The Arrhenius plot in figure 3(b) suggests $2\Delta_{\mathrm{act}} \approx 0.8$ eV, but the data are not very well described by simple activated behavior. The data are best described by the non-adiabatic small-polaron model [42], predicting $\rho = CT^{3/2}\exp(\Delta_{\mathrm{act}}/(k_{\mathrm{B}}T))$ (see figure 3(b)). Within this model we obtain $2\Delta_{\mathrm{act}} = 0.78$ eV, in agreement with both the estimate based on simple activated behavior and in particular with the onset of absorption observed in $\sigma(\omega)$ (see top panel of figure 2). This value is significantly larger than reported in [41], demonstrating the high quality of our samples. Remarkably, DFT–PIRG calculations [32] predict an indirect gap at 0.7 eV, in excellent agreement with our data. Altogether, we have strong evidence that all absorption features observed in $\sigma(\omega)$ below 0.8 eV arise from phonons, magnons, excitons or orbital excitations.

The optical conductivity of YVO_3 below 0.9 eV is given in figure 4. The absorption due to phonons gives rise to the steep increase of $\sigma(\omega)$ below about 80 meV, in agreement with the data reported in [27]. Thus, weak two-phonon features can be observed up to about 160 meV, whereas

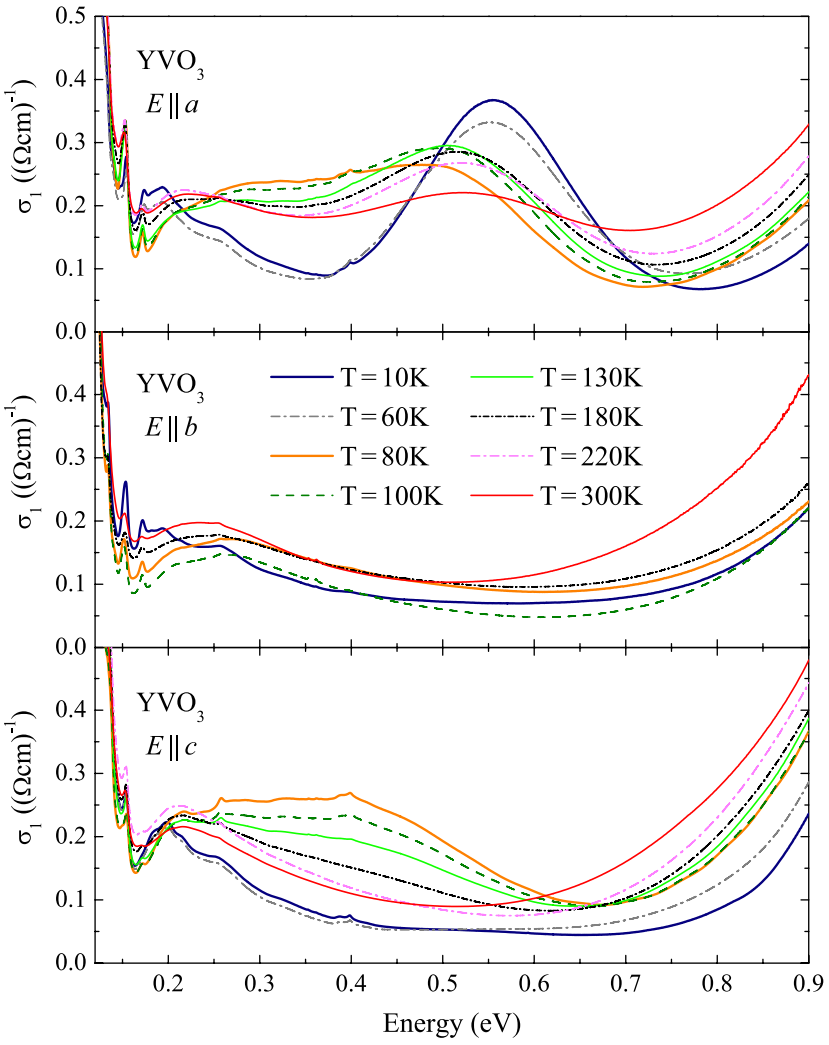

Figure 4. Temperature dependence of $\sigma(\omega)$ of YVO_3 in the mid-infrared range for $E \parallel a$ (top panel), $E \parallel b$ (middle), and $E \parallel c$ (bottom). The features at 0.4 eV for $E \parallel c$ and 0.55 eV for $E \parallel a$ constitute our main experimental result.

three-phonon absorption is expected to be still much weaker. A contribution to $\sigma(\omega)$ from spin waves may arise in the form of two-magnon-plus-phonon absorption [43, 44]. However, in YVO_3 the spin-wave dispersion does not exceed 40 meV [34]. Thus, a possible two-magnon-plus-phonon contribution is expected to peak below 0.2 eV and clearly is not related to the features observed above 0.2 eV.

As far as excitons are concerned, we have to distinguish between strongly and weakly bound excitons. In a Mott–Hubbard insulator, an exciton is a bound state of an electron in the upper Hubbard band (i.e. a double occupancy) and a hole in the lower Hubbard band (an 'empty site'). In the case of a weakly bound exciton, the electron and the hole occupy distinct sites, e.g. nearest-neighbor sites. The binding may result from the nearest-neighbor Coulomb attraction. Recently, an excitonic resonance was reported [45] in the orbitally ordered $3d^1$ Mott–Hubbard insulator $YTiO_3$ at 1.95 eV. We consider it as unrealistic to assume a binding energy large enough to pull such a weakly bound exciton far below 1 eV in YVO_3. Moreover,

the spectral weight of the exciton in $YTiO_3$ is more than two orders of magnitude larger than the spectral weight between 0.1 and 0.7 eV in YVO_3.

3.1. Orbital excitations

The physics is different for a strongly bound exciton, in which case the electron and the hole share the $3d$ shell of the *same* site. This actually corresponds to an orbital or d–d excitation (or to a spin excitation, which has been ruled out above). These excitations may occur far below the gap because the binding energy and the gap are both of the order of the on-site Coulomb repulsion U. In other words, double occupancy is omitted if the electron and the hole share the same site, thus one does not have to pay the energy U. Orbital excitations in the form of local CF excitations are a common feature in many transition-metal compounds in the considered frequency range [7]–[9]. The central question to us is whether the observed orbital excitations are such local crystal-field excitations or propagating orbitons, reflecting the importance of orbital exchange interactions. The orbiton dispersion for orbitally ordered vanadates has been investigated theoretically [13]. Predictions for Raman scattering [13, 16, 17] and inelastic neutron scattering [13] have been discussed, but contributions to $\sigma(\omega)$ for the case of dominant exchange interactions have not been considered thus far. Moreover, a quantitative description requires that both the exchange interactions and the coupling to the lattice are treated on the same footing [46, 47], but up to now such calculations have not been reported for the vanadates. Therefore, we first compare our results with the expectations for local CF excitations of $3d^2$ V^{3+} ions. We use VOCl as a typical example for the absorption spectrum of V^{3+} ions in a predominantly octahedral, but distorted environment (see bottom panel of figure 2). In the sister compound TiOCl, the orbital excitations are very well described in terms of local CF excitations [9, 48].

YVO_3 shows inversion symmetry on the V sites, thus local CF excitations are not infrared-active due to the parity selection rule. However, they become weakly allowed by the simultaneous excitation of a symmetry-breaking phonon [7]–[9]. In VOCl (*Pmmn*) there is no inversion symmetry on the V site [49] and the CF excitations are weakly allowed without the additional excitation of a phonon.[8]

For the sake of simplicity, we start from an undistorted octahedral crystal field, the effect of a lower symmetry will be discussed below. The ground state of a d^2 system in an octahedral field is the nine-fold degenerate ${}^3T_1$ level with total spin $S = 1$, in which two electrons with parallel spins occupy the t_{2g} level, $t_{2g}^{\uparrow\uparrow}$ [7]. The splitting between t_{2g} and e_g levels typically amounts to $\gtrsim 2$ eV for O^{2-} ligands [7, 8]. For VOCl, this splitting is reduced due to the smaller ligand strength of the Cl^- ions and can be identified with the feature observed around 1.7 eV (see bottom panel of figure 2). For YVO_3, it is reasonable to assume that the t_{2g}–e_g splitting is larger than the Mott–Hubbard gap. In the following, we focus on the excitations within the t_{2g} shell, which are located at lower energies.

In an octahedral field, the spin–flip excitation from the ${}^3T_1$ ground state with $S = 1$ to the five-fold degenerate $S = 0$ state $({}^1T_2, {}^1E; t_{2g}^{\uparrow\downarrow})$ occurs at $2J_H$. The Hund exchange $J_H \approx 0.7$ eV [51] is hardly screened in a solid, therefore this excitation is observed at very similar energies in different V compounds [52]–[54], irrespective of the crystal structure. Typical examples are the weak, sharp features observed between 1.1 and 1.3 eV in VOCl

[8] Raman data of the phonons in VOCl indicate a lower local symmetry on the V site [50]. However, in our context this affects just details of the spectrum, i.e. the number of spin-forbidden excitations.

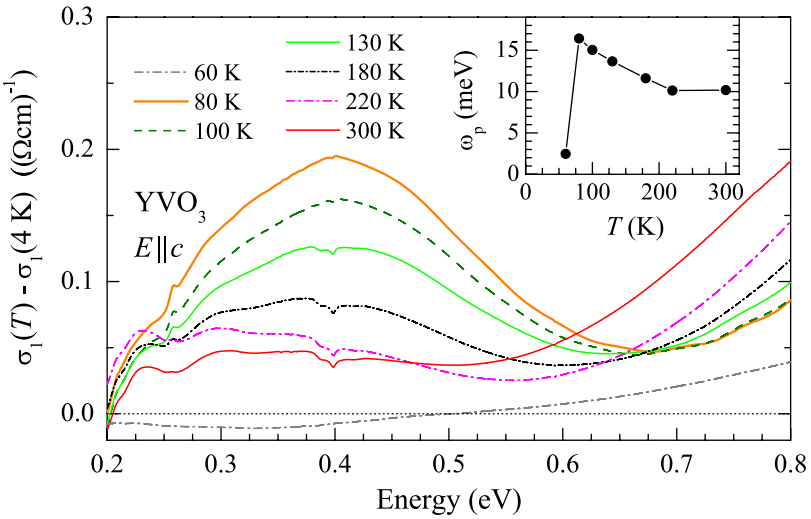

Figure 5. Spectral weight and line shape of the peak at 0.4 eV for $E \parallel c$ in YVO_3. According to our microscopic model, the two-orbiton excitation is forbidden below $T_S = 77$ K. Therefore, the data for 4 K have been subtracted for each temperature as an estimate for the background of, e.g. multi-phonon absorption. The inset depicts the plasma frequency ω_p (see equation (8)) for $\omega_{lo} = 0.20$ eV and $\omega_{hi} = 0.68$ eV.

(see bottom panel of figure 2). These spin–flip excitations are very weak due to the spin-selection rule, they become weakly allowed by spin–orbit coupling or by the simultaneous excitation of a magnon [7]. Such spin-flip bands often are very sharp because the orbital occupation stays the same, thus the coupling to the lattice is only weak (the large width of spin-allowed excitations is attributed to vibronic Franck–Condon sidebands). Also in YVO_3, sharp features are observed between 1.1 and 1.4 eV which can be attributed to spin-forbidden excitations. The oscillator strength is clearly enhanced compared with VOCl. Presumably, this is due to the overlap with the onset of excitations across the Mott–Hubbard gap. Mixing the two kinds of excitations will transfer some weight to the orbital bands, a process called 'intensity stealing'.

In a local CF scenario, all features observed significantly below 1 eV have to be interpreted as spin–conserving transitions within the t_{2g} shell, i.e. both the ground state and the excited state show $S = 1$. Both in YVO_3 and in VOCl, the symmetry on the V sites is lower than tetragonal, thus the t_{2g} level is split into three distinct orbitals. For two electrons with parallel spins, there are three distinct energy levels, each showing three-fold spin degeneracy. In strongly distorted VOCl, we observe the corresponding excitations at 0.3–0.4 eV (see figure 2). For YVO_3, one expects lower excitation energies because the distortions away from an octahedral environment are smaller than in VOCl. Indeed, recent first-principles [21] and LDA+DMFT calculations [15] predict intra-t_{2g} excitations in YVO_3 in the range of 0.10–0.20 eV and 0.06–0.24 eV, respectively. Our data of $\sigma(\omega)$ of YVO_3 show an absorption band centered around 0.20–0.25 eV at all temperatures and for all polarization directions (see figure 4), in agreement with these expectations.

Our main experimental result is the observation of the two remaining features which *cannot* be explained within a local CF scenario, namely the peaks at about 0.4 eV for $E \parallel c$ and at 0.55 eV for $E \parallel a$ (see figures 4 and 5). As follows from the discussion above, these features are

hard to reconcile with a local CF scenario: the energy is too low for a spin–flip transition and too high for a spin-conserving intra-t_{2g} transition. Moreover, the strong polarization dependence of both peaks is entirely unexpected for a phonon-assisted CF excitation. Since the phonon polarization is arbitrary, one does not expect strict polarization selection rules [9]. Even in VOCl, where CF excitations are directly allowed, the absorption is very similar for the two polarization directions. Finally, also the pronounced temperature dependence is unexpected for a local CF excitation. For $E \parallel c$, the spectral weight around 0.4 eV is independent of temperature for $T > T_{OO} = 200$ K, increases with decreasing temperature below T_{OO}, and abruptly disappears at $T_S = 77$ K (see inset of figure 5). For a local CF excitation, both the spectral weight and the energy in principle may change across a structural phase transition. However, LDA+DMFT calculations [15] predict that the intra-t_{2g} excitation energies change by less than 40 meV across T_S, thus the abrupt change of $\sigma(\omega)$ at T_S cannot be explained.

3.2. Orbitons

Thus far, we have neglected the exchange interactions between orbitals on neighboring sites, which change the character of the excitations from 'local' CF excitations to propagating orbitons. Here, we consider two different processes for the excitation of orbitons [13]. Firstly, the excitation process itself may be based on the exchange of orbitals between adjacent sites (see below). Secondly, an orbiton may be excited *locally* by flipping an orbital on a single site, e.g. from xz to yz, with subsequent propagation of the orbital flip. In the latter case, the excitation process is as discussed above in the local CF limit, i.e. it requires the simultaneous excitation of a symmetry-breaking phonon to obtain a finite dipole moment for the local orbital flip. The difference arises from the propagation of the orbital flip, which is similar to a spin flip which translates into a spin wave or magnon in a system with long-range magnetic order. For such a propagating orbital flip, we have to take into account the dispersion. Due to momentum conservation, $\sigma(\omega)$ is sensitive to excitations with $\Delta\mathbf{k}_{tot} = 0$, where $\Delta\mathbf{k}_{tot} = \mathbf{k}_{phonon} + \mathbf{k}_{orbiton}$. Since the symmetry-breaking phonon may have any momentum, $\sigma(\omega)$ reflects orbiton contributions from the entire Brillouin zone. However, without more detailed theoretical predictions about the line shape or width, this one-orbiton-plus-phonon peak cannot be distinguished from the broad vibronic Franck–Condon peak expected in the local CF limit. Thus, we can attribute the absorption feature around 0.2 eV to a single orbital flip, but we cannot decide whether this flip is only local or propagates due to orbital exchange interactions. In principle, the dispersion can be significant if the exchange coupling is large and the CF splitting is small [13, 16, 17, 46, 47]. In comparison to e_g systems, the exchange coupling is smaller in t_{2g} systems, but this may be overcompensated by a reduced CF splitting. As mentioned in the introduction, it has been discussed controversially whether the exchange interactions or the CF splitting dominate in YVO_3 [14, 15, 31], [34]–[37].

In the other case mentioned above, the excitation process is based on the exchange of orbitals between adjacent sites [19]. Here, we primarily focus on the peak for $E \parallel c$ at 0.4 eV. Our interpretation of this feature as a two-orbiton excitation naturally explains its energy, the polarization dependence, and the pronounced temperature dependence, i.e. it resolves the three issues mentioned above. For the exchange along the c axis, we consider only the dominant processes and neglect the rotation and tilt distortions of the octahedra. In this case, hopping preserves the type of orbital, i.e. the only finite hopping processes are $xz(\alpha) \leftrightarrow xz(\beta)$ and $yz(\alpha) \leftrightarrow yz(\beta)$, where α and β denote neighboring V(1) and V(2) sites, respectively

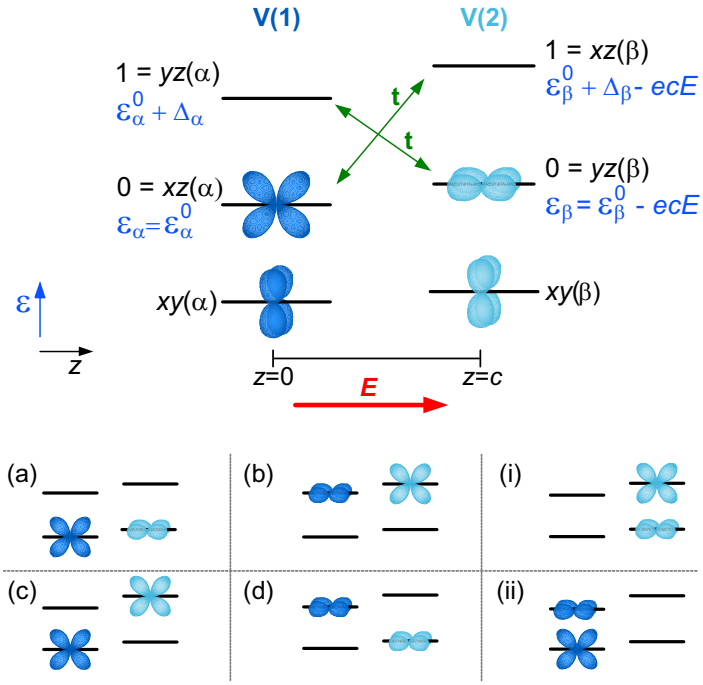

Figure 6. Top: Sketch of the local energy levels and of the hopping processes between neighboring V sites for the two-orbiton excitation in the monoclinic phase of $R\mathrm{VO}_3$ with an electric field E applied parallel to the c-axis. Only xz and yz orbitals are considered for the exchange because the lower-lying xy orbital is always occupied by one electron. The spin is omitted since we consider fully polarized electrons. See text for more details. Bottom: For two electrons with parallel spins, there are six possibilities to occupy the xz and yz orbitals on sites V(1) and V(2): (a) orbital ground state; (b) two-orbiton excited state; (c) and (d) one-orbiton excited states; (i) and (ii) states in the upper Hubbard band with a doubly occupied V site.

(see figure 6). Note that hopping in the z-direction is zero for the xy orbital, which is the lowest orbital on all sites and thus occupied by one electron. Following the analysis of synchrotron x-ray data by Noguchi *et al* [28], we consider G-type OO for the intermediate phase (see figure 1), i.e. the second electron per site occupies xz on V(1) and yz on V(2) in the ground state. For this second electron per site, we consider the fermionic Hamiltonian H_F

$$H_\mathrm{F} = H_{\mathrm{F}0} + t(c^\dagger_{\alpha 1} c_{\beta 0} + c^\dagger_{\alpha 0} c_{\beta 1} + \mathrm{h.c.}), \tag{1a}$$

$$H_{\mathrm{F}0} = \sum_{\tau \in \{\alpha,\beta\}} \left((\varepsilon_\tau + \Delta_\tau) c^\dagger_{\tau 1} c_{\tau 1} + \varepsilon_\tau c^\dagger_{\tau 0} c_{\tau 0} + U' c^\dagger_{\tau 1} c_{\tau 1} c^\dagger_{\tau 0} c_{\tau 0} \right), \tag{1b}$$

where t denotes the hopping matrix element, $c^\dagger_{\tau i}$ ($c_{\tau i}$) creates (annihilates) an electron in orbital $i = 0$ or 1 on site $\tau \in \{\alpha, \beta\}$, $U' = U - 3J_\mathrm{H}$ denotes the Coulomb repulsion for two electrons on the same site but in different orbitals, and the energies ε_τ and Δ_τ are illustrated in figure 6. No spin appears since we consider parallel spins due to Hund's coupling to the electron in the xy orbital. In the orbital ground state, the lower levels (denoted 0) are occupied by one electron,

the upper levels (denoted 1) are empty. The creation of an orbiton at site τ corresponds to the excitation of an electron from 0 to 1 at τ, which requires the energy Δ_τ. We introduce bosonic orbiton creation operators $b_\tau^\dagger$ with

$$b_\tau^\dagger := c_{\tau 1}^\dagger c_{\tau 0}. \tag{2}$$

The annihilation operators are the Hermitean conjugate ones. Note that the orbitons are hardcore bosons since at maximum there can be only one at each site.

In the second order in t the orbital ground state of H_F (state (a) in figure 6) is linked via the intermediate states (i) or (ii) to state (b) with *two* excited orbitons, one at site α and one at site β. Note that states (c) and (d) corresponding to the excitation of a single orbiton cannot be reached from the ground state in the considered symmetry[9]. In contrast, the two-orbiton excitation can account for the observed energy, polarization and temperature dependence. For the energy of a two-orbiton excitation, one roughly expects twice the energy of a one-orbiton excitation, neglecting orbiton–orbiton interactions and kinetic effects. As discussed above, single orbital excitations are observed around 0.2 eV, hence the energy of the feature at 0.4 eV is well described by a two-orbiton interpretation. Due to Hund's coupling with the electron in the low-lying xy orbital, this two-orbiton excitation requires parallel alignment of the spins on the considered bond, which in YVO_3 is only present in the intermediate phase and only along the c-axis, in agreement with the observed polarization and temperature dependence. Moreover, the two-orbiton excitation requires hopping from, e.g. xz on V(1) to xz on V(2), thus the spectral weight becomes zero if both orbitals are occupied in the ground state. This is the case for the C-type OO observed below T_S, explaining the abrupt drop of the intensity at T_S (see figure 5). For the intermediate phase, we have assumed pure G-type OO for simplicity, neglecting admixtures of C-type (see discussion in the introduction). Note that deviations from G-type OO as claimed recently on the basis of LDA+DMFT calculations [15] will only affect the precise value of the spectral weight. In order to understand the temperature dependence at higher temperatures, we now address the dipole-selection rule and calculate the spectral weight of this two-orbiton excitation.

In analogy to the derivation of Heisenberg exchange, we derive an effective Hamiltonian H_orb in terms of orbiton creation and annihilation operators for the mixture of states (a) and (b)

$$H_\mathrm{orb} = J(b_\alpha^\dagger b_\beta^\dagger + \mathrm{h.c.}) + \mathrm{const.} \tag{3}$$

In this effective description no virtual double occupancies appear. To do so, we assume that the on-site Coulomb interaction is the largest energy

$$U' > |\varepsilon_\alpha + \Delta_\alpha - \varepsilon_\beta|, \tag{4a}$$

$$U' > |\varepsilon_\beta + \Delta_\beta - \varepsilon_\alpha|. \tag{4b}$$

This assumption is certainly met in YVO_3, where $U' = U - 3J_\mathrm{H} \approx 2\,\mathrm{eV}$ and all other energies are of the order of fractions of 1 eV. We find (see the appendix)

$$J = \frac{2t^2 U'}{(U')^2 - (\delta - ecE)^2}, \tag{5}$$

[9] From the ground state (a), the one-orbiton states (c) and (d) can only be reached if the off-diagonal hopping $xz(\alpha) \leftrightarrow yz(\beta)$ is finite, i.e. it requires deviations from the ideal perovskite structure.Therefore, the matrix element is significantly smaller than for the two–orbiton excitation.

where e is the elementary charge, c is the distance between the two sites, E denotes an electric field applied parallel to the bond along the c-axis, and

$$\delta = \varepsilon_\beta^0 - \varepsilon_\alpha^0 + \frac{\Delta_\beta - \Delta_\alpha}{2} = (\varepsilon_\beta^0 + \varepsilon_\beta^1 - \varepsilon_\alpha^0 - \varepsilon_\alpha^1)/2, \tag{6}$$

where $\varepsilon_\tau^1 = \varepsilon_\tau^0 + \Delta_\tau$ (see figure 6). The two-orbiton excitation is dipole allowed if $\partial H_{\rm orb}/\partial E \neq 0$. We find

$$\partial J/\partial E \approx -\frac{4t^2}{(U')^3}\,\delta\, ec. \tag{7}$$

In the denominator, we neglected δ because it is much smaller than U'.

In the presence of a mirror plane between the two V sites, i.e. $\varepsilon_\beta^0 = \varepsilon_\alpha^0$ and $\Delta_\beta = \Delta_\alpha$, the two-orbiton excitation does not carry a dipole moment and does not contribute to $\sigma(\omega)$. However, such a mirror plane is present only below $T_{\rm S} = 77\,{\rm K}$ and above $T_{\rm OO} = 200\,{\rm K}$, but the symmetry is broken in the intermediate phase with two distinct V sites. The situation is similar to the case of two-magnon absorption discussed by Lorenzana and Sawatzky [43, 44]. They demonstrated that two-magnon absorption becomes weakly infrared active if the mirror symmetry on the bond is broken by the simultaneous excitation of a phonon. In the present case, the symmetry is already broken without a phonon. We conclude that the excitation of two orbitons is directly infrared active for $E \parallel c$ in the intermediate, monoclinic phase of YVO_3.

The absolute value of $\partial J/\partial E$ depends on the CF levels via δ. From the first-principles study by Solovyev [21] and the LDA+DMFT calculation by De Raychaudhury *et al* [15] we obtain $\delta = 20$ and 33.5 meV, respectively. However, each individual level ε_τ^i certainly is known only with an accuracy of 50 meV, thus the error of δ is about 100 meV. For $U' = 2\,{\rm eV}$, $\delta = 20$–$100\,{\rm meV}$, and $t = 100$–$150\,{\rm meV}$ [15] we obtain $\partial J/\partial E = 0.1$–$1.1 \times (10^{-3}\, ec)$. The spectral weight usually is expressed in terms of the plasma frequency $\omega_{\rm p}$,

$$\int_{\omega_{\rm lo}}^{\omega_{\rm hi}} \sigma_1(\omega)\,{\rm d}\omega = \frac{\pi\,\varepsilon_0}{2}\omega_{\rm p}^2, \tag{8}$$

where the frequency range of interest is defined by $\omega_{\rm lo}$ and $\omega_{\rm hi}$, and ε_0 denotes the dielectric constant of vacuum. The spectral weight of the two-orbiton excitation at $\hbar\omega_{2{\rm o}} = 0.4\,{\rm eV}$ is given by

$$\omega_{\rm p}^2 = \frac{2\omega_{2{\rm o}}}{\hbar\varepsilon_0 V}|\partial J/\partial E|^2, \tag{9}$$

where $V = 56\,{\rm \AA}^3$ is the volume per site. Finally, we obtain $\hbar\omega_{\rm p} = 0.6$–$6.8\,{\rm meV}$. This has to be compared with the experimental result for the spectral weight, for which we choose $\hbar\omega_{\rm lo} = 0.20\,{\rm eV}$ and $\hbar\omega_{\rm hi} = 0.68\,{\rm eV}$. In order to separate the two-orbiton contribution from a background of, e.g. multi-phonon absorption, the integration for each temperature T is performed over $\sigma_1(T,\omega) - \sigma_1(4{\rm K},\omega)$, since the two-orbiton excitation is not dipole allowed at 4 K (see figure 5). At 80 K this yields $\hbar\omega_{\rm p}^{\rm exp} = 16\,{\rm meV}$, about a factor of 2–26 larger than the calculated result. We emphasize that the quantitative prediction of the spectral weight is a challenging task. Note that the theoretical estimate of $\omega_{\rm p}$ of the phonon-assisted two-magnon absorption in the cuprates on the basis of a similar perturbation expansion was off by a factor of 4–7 [43, 55]. Therefore, we consider this result as a clear support for our interpretation.

The temperature dependence of $\omega_{\rm p}$ is plotted in the inset of figure 5. Upon warming above $T_{\rm OO} = 200\,{\rm K}$, the mirror plane is restored and the direct contribution to $\sigma(\omega)$ is suppressed. However, the spectral weight above $T_{\rm OO}$ is larger than at 10 K. This may either arise from a

weak, phonon-assisted two-orbiton contribution or from thermal broadening of the electronic gap and of the absorption band around 0.2 eV (see figure 5). In the case of phonon-assisted two-*magnon* absorption proposed by Lorenzana and Sawatzky [43], $\sigma(\omega)$ in low-dimensional antiferromagnets is hardly affected at the magnetic ordering temperature T_N, because the spin–spin correlation length remains large above T_N. In YVO_3, measurements of the specific heat [22] show that only of the order of 10% of the expected entropy are released in the phase transition at T_{OO}, which indicates strong fluctuations. Therefore, a finite contribution of phonon-assisted two-orbiton excitations is possible above T_{OO}. In contrast, the spectral weight abruptly vanishes upon cooling below $T_S = 77$ K, because the mirror symmetry is restored and because both the orbital and the magnetic ordering patterns change (see figure 1). The reduction of $\hbar\omega_p$ from 16 to 10 meV observed between T_S and T_{OO} can tentatively be attributed both to a reduction of ferromagnetic correlations between nearest neighbors above T_N and to rather small changes of the orbital occupation or of the CF levels. For $\delta = 20$–100 meV, a reduction of ω_p by a factor of 1.6 corresponds to changes of the four individual CF levels of only about 4–20 meV.

The line shape, in principle, may serve as a key feature to test our interpretation. However, this requires one to take into account the orbital exchange interactions and the coupling to the lattice on the same footing [46]. On top of that, orbiton–orbiton interactions also have to be considered. Up to now, theoretical predictions for the two-orbiton contribution to $\sigma(\omega)$ have not been available. Due to momentum conservation, $\sigma(\omega)$ is restricted to the observation of two-orbiton processes with $\mathbf{k}_{tot} = \mathbf{k}_1 + \mathbf{k}_2 \approx 0$. This means that the two orbitons have opposite momenta $\mathbf{k}_1 = -\mathbf{k}_2$ with arbitrary $\mathbf{k}_i$, and thus the orbiton dispersion is probed throughout the entire Brillouin zone. The total line width is a convolution of twice the orbiton bandwidth and the width arising from vibronic coupling to the lattice.

In order to test our interpretation of the feature in YVO_3 at 0.4 eV for $E \parallel c$, we study $HoVO_3$, which shows a very similar crystal structure and very similar magnetic and orbital ordering patterns. The absorption coefficient $\alpha(\omega) \propto -\ln(T(\omega))/d$ of $HoVO_3$ shows qualitatively the same mid-infrared features as observed in YVO_3, i.e. a peak at 0.4 eV for $E \parallel c$ in the intermediate phase, and a peak at about 0.55 eV for $E \parallel a$ in the whole temperature range with the same anisotropy between $\sigma_a(\omega)$ and $\sigma_b(\omega)$ (see figure 7). In $HoVO_3$, the phase transitions occur at $T_S \sim 40$ K and $T_{OO} \sim 188$ K [38]. Additionally, an absorption band consisting of several sharp lines is observed around 0.64 eV, which can be attributed to the f–f transitions of the Ho^{3+} ion ($^5I_8 \rightarrow {}^5I_7$). The fine structure of this band is due to transitions between different Stark components. Note that the polarization of the incident light mainly affects the intensity of the observed lines. The close similarity of the spectra of YVO_3 and $HoVO_3$ regarding the orbital excitations within the $3d$ shell and in particular the sensitivity to the phase transitions clearly show that the considered features reflect intrinsic properties of the vanadates and corroborate our interpretation. It is tempting to speculate about the implications for other rare earth vanadates, in particular for those with larger ionic radii such as $LaVO_3$ or $CeVO_3$. These exhibit the monoclinic phase with G-type OO and C-type SO down to low temperatures. The LDA+DMFT study by De Raychaudhury *et al* [15] predicts that the CF splitting is significantly smaller in $LaVO_3$ compared to YVO_3, and that quantum orbital fluctuations are strong in the high-temperature orthorhombic phase of $LaVO_3$, but suppressed in the monoclinic phase. Our microscopic model refers to G-type OO with C-type SO. On this basis, we predict similar features to be found in all RVO_3 compounds. We expect that the dependence of the energy, line width, shape and spectral weight on the details of the lattice distortions, i.e. on the R ions, will help to further elucidate the character of the

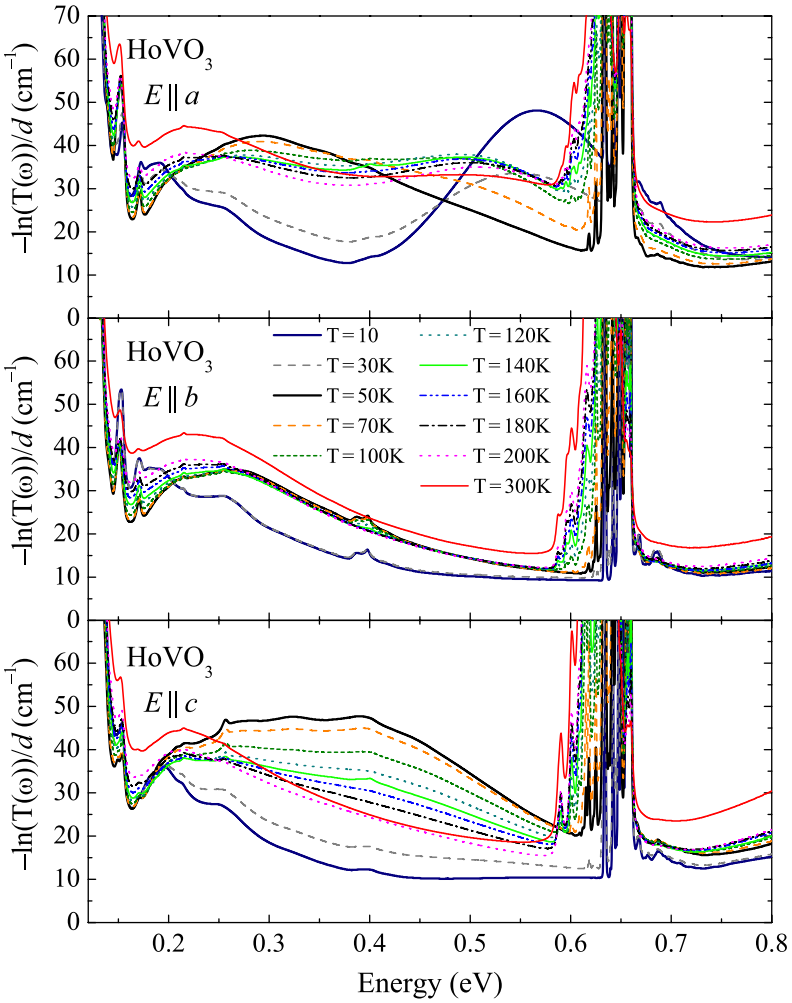

Figure 7. Temperature dependence of $-\ln(\mathrm{T}(\omega))/d$ of $HoVO_3$ for $E \parallel a$ (top panel), $E \parallel b$ (middle) and $E \parallel c$ (bottom). The band of sharp lines at 0.6 eV originates from CF excitations within the Ho $4f$ shell.

orbital excitations in these compounds. In particular, it is very promising to find out how the pronounced temperature dependence of the peak position and line shape observed for $E \parallel a$ in the monoclinic phase of $HoVO_3$ (see figures 8 and 9) behaves at still lower temperatures in the monoclinic phase of $LaVO_3$.

What are the implications of our results for the claimed observations of orbitons by Raman scattering [16]–[18] at energies of the order of 40–80 meV (see the introduction)? The excitation energy of 0.4 eV for $E \parallel c$ implies that $\Delta_\alpha + \Delta_\beta \approx 0.4$ eV. This may be consistent with a comparably small one-orbiton energy if the CF splitting on V(1) and V(2) differs substantially, e.g. $\Delta_\alpha = 50$–100 meV and $\Delta_\beta = 300$–350 meV. Note that a rather large value of $|\Delta_\beta - \Delta_\alpha|$ is in agreement with the observed value of the spectral weight (see above). However, the spectra for $E \parallel b$ indicate that both Δ_α and Δ_β are smaller than 300 meV, implying $100\,\mathrm{meV} < \Delta_\tau < 300\,\mathrm{meV}$.

Finally, we turn to the feature at 0.55 eV for $E \parallel a$. Its rather high energy suggests that excitations from the low-lying xy orbital are involved. At all temperatures studied here, there

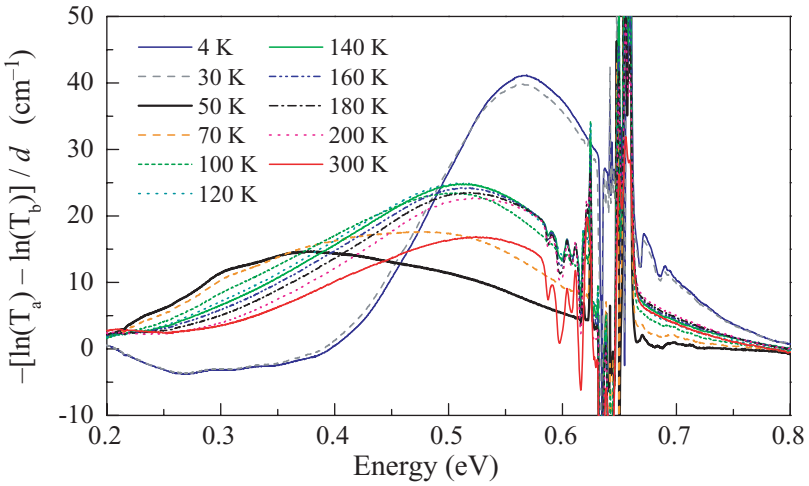

Figure 8. Anisotropy of the absorption spectra for $E \parallel a$ and $E \parallel b$ for $HoVO_3$.

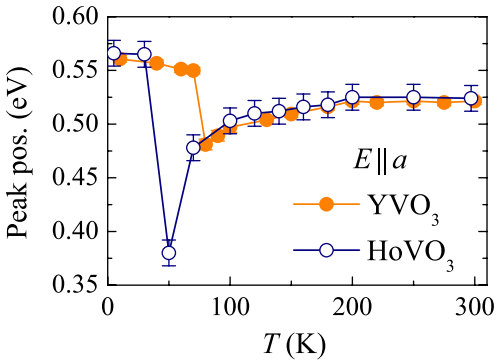

Figure 9. Peak frequency observed for $E \parallel a$ in YVO_3 and $HoVO_3$.

is no significant contribution to $\sigma_b(\omega)$ around 0.5 eV (see figures 4 and 7). This pronounced anisotropy puts severe constraints on the interpretation. Assuming an ideal perovskite structure, one expects $\sigma_a(\omega) = \sigma_b(\omega)$. In YVO_3 and $HoVO_3$, the V–O–V bonds are rotated within the ab-plane by about 45° with respect to the orthorhombic a- and b-axes, with antiferro-orbital ordering in the entire temperature range (see figure 1). Therefore, one expects that an exchange process between *neighboring* V sites contributes roughly equally to $\sigma_a(\omega)$ and $\sigma_b(\omega)$. In contrast, *next-nearest* V neighbors are displaced parallel to the a- or b-axis. One may speculate that the structural distortions, i.e. rotations and tilts of the octahedra, give rise to the observed anisotropy. Such a detailed theoretical analysis of the exchange between next-nearest neighbors including structural details is beyond the scope of the present paper. In order to highlight the anisotropy and to obtain a better view of the line shape, we plot the difference spectra between a- and b-axis of $HoVO_3$ in figure 8. The temperature dependence of the peak frequency is shown in figure 9. Upon cooling down from 300 K, the peak position, spectral weight and line shape all change below about 100 K. This is more evident in $HoVO_3$, because the change is cut off at the first-order transition at T_S, which is higher in YVO_3. Possibly, this may be related to the Neél temperature, $T_N = 116$ K in YVO_3 and 114 K in $HoVO_3$ [38]. This points towards the entanglement of spin and orbital degrees of freedom, which is expected if exchange interactions are dominant [56].

4. Conclusion

In conclusion, the orbital excitations in YVO_3 and $HoVO_3$ have been studied by optical spectroscopy. We have focused on an absorption band observed at 0.4 eV for $E \parallel c$. We have shown that this feature is located far below the Mott–Hubbard gap and that it can neither be interpreted in terms of phonons, magnons, weakly bound (Mott–Hubbard) excitons, nor be polaronic carriers trapped at impurity sites. Therefore, we identify this feature as an orbital excitation. However, based on the comparison with the data of VOCl and with recent calculations [15, 21], we have shown that this absorption peak cannot be explained in a local CF scenario, i.e. within single-site physics. Alternatively, we propose that this peak reflects collective orbital excitations, i.e. orbital excitations that are based on the exchange coupling between neighboring V sites. We demonstrate that the exchange of two orbitals between adjacent sites along the c-axis in the intermediate phase directly contributes to $\sigma(\omega)$. The energy, polarization and temperature dependence as well as the spectral weight of the absorption band at 0.4 eV are in excellent agreement with the expectations for a two-orbiton excitation.

Our results call for a number of further investigations. Our claim can be tested directly by the direct observation of the dispersion with a momentum-resolving technique such as resonant inelastic x-ray scattering or electron energy loss spectroscopy. Moreover, we call for theoretical studies of the orbital exchange that realistically take into account the coupling to the lattice. In particular, a comparison of our data with predictions for the line shape of two-orbiton absorption is expected to reveal important information on orbital–orbital interactions. Finally, more detailed investigations of the exchange between next-nearest neighbors within the ab-plane are necessary to clarify the nature of the absorption band observed at 0.55 eV for $E \parallel a$.

Acknowledgments

It is a pleasure to acknowledge fruitful discussions with D I Khomskii, M Mostovoy, and P van Loosdrecht. This project is supported by the DFG via SFB 608.

Appendix

Here, we discuss the derivation of the effective Hamiltonian $H_{\rm orb}$ (see equation (3)). Conceptually, this is even in second order less trivial than one might think at first glance. This is so because the states without double occupancy (states (a) and (b) in figure 6) are not degenerate due to the differences in the energies ε_τ and Δ_τ. This leads to the remarkable phenomenon that different second-order calculations lead to different results. This stems from the different ways to perform the unitary transformation which eliminates the terms which change the number of double occupancies. Similar observations were made previously in the derivation of the electron–electron attraction mediated by phonons [57]. We illustrate this issue here by two calculations.

Both the calculations require splitting the hopping part of $H_{\rm F}$ (second term in equation (1a)) into two parts

$$t(c^\dagger_{\alpha 1}c_{\beta 0} + c^\dagger_{\alpha 0}c_{\beta 1} + \text{h.c.}) = H_{\rm F+} + H_{\rm F-} \tag{A.1}$$

with $H_{\rm F-} = (H_{\rm F+})^\dagger$ and $H_{\rm F+} = H_{\rm F++} + H_{\rm F-+}$. The first plus (minus) sign indicates that a double occupancy is created (annihilated). The second sign indicates whether an electron is raised (+) or lowered (−), i.e. hops from 0 to 1 (+) of vice versa (−). This implies $H_{\rm F-+} = (H_{\rm F+-})^\dagger$ and

$H_{\mathrm{F}--} = (H_{\mathrm{F}++})^\dagger$. In detail, we have

$$H_{F++} = t(c^\dagger_{\alpha 1} c_{\beta 0} \hat{n}_{\alpha 0} + c^\dagger_{\beta 1} c_{\alpha 0} \hat{n}_{\beta 0}), \tag{A.2a}$$

$$H_{F+-} = t(c^\dagger_{\alpha 0} c_{\beta 1} \hat{n}_{\alpha 1} + c^\dagger_{\beta 0} c_{\alpha 1} \hat{n}_{\beta 1}). \tag{A.2b}$$

A.1 Standard unitary transformation

The standard approach is to determine an anti-Hermitean operator $\eta = \eta_+ - \eta_-$ such that

$$H_{\mathrm{orb}} = \exp(\eta) H_{\mathrm{F}} \exp(-\eta) \tag{A.3}$$

holds. To eliminate the hopping in leading order, we require $[\eta, H_{\mathrm{F}0}] = -H_{\mathrm{F}+} - H_{\mathrm{F}-}$ which leads to

$$\eta_{++} = \frac{t c^\dagger_{\alpha 1} c_{\beta 0} \hat{n}_{\alpha 0}}{U' + \Delta_\alpha - \Delta\varepsilon} + \frac{t c^\dagger_{\beta 1} c_{\alpha 0} \hat{n}_{\beta 0}}{U' + \Delta_\beta + \Delta\varepsilon}, \tag{A.4a}$$

$$\eta_{+-} = \frac{t c^\dagger_{\alpha 0} c_{\beta 1} \hat{n}_{\alpha 1}}{U' - \Delta_\beta - \Delta\varepsilon} + \frac{t c^\dagger_{\beta 0} c_{\alpha 1} \hat{n}_{\beta 1}}{U' - \Delta_\alpha + \Delta\varepsilon}, \tag{A.4b}$$

where we used $\Delta\varepsilon = \varepsilon_\beta - \varepsilon_\alpha$, and $\eta_+ = \eta_{++} + \eta_{+-}$ as for the parts of the Hamiltonian, with $\eta_- = \eta_{--} + \eta_{-+}$, $\eta_{--} = (\eta_{++})^\dagger$, and $\eta_{-+} = (\eta_{+-})^\dagger$. In the second order in $t/\mathcal{O}(U')$, we obtain $H_{\mathrm{orb}} = \frac{1}{2}[\eta, H_{\mathrm{F}+} + H_{\mathrm{F}-}]$. Using the shorthand $H_{\mathrm{orb}+} = J b^\dagger_\alpha b^\dagger_\beta$ for the creation of two orbitons, we have to compute

$$H_{\mathrm{orb}+} = (1/2)\left([\eta_{++}, H_{\mathrm{F}-+}] + [H_{\mathrm{F}++}, \eta_{-+}]\right). \tag{A.5}$$

Explicit commutation leads to the standard result

$$J_{\mathrm{stan}} = \frac{t^2 U'}{(U')^2 - (\Delta_\alpha - \Delta\varepsilon)^2} + \frac{t^2 U'}{(U')^2 - (\Delta_\beta + \Delta\varepsilon)^2}. \tag{A.6}$$

For $\Delta_\tau = 0 = \Delta\varepsilon$ this is identical to the result known from the derivation of the Heisenberg spin exchange as in $(J_{\mathrm{Heisen}}/2)(S^+_\alpha S^-_\beta + S^-_\alpha S^+_\beta)$ which implies $2J = J_{\mathrm{Heisen}} = 4t^2/U'$. Note that equation (A.6) for the exchange J becomes singular as soon as $U' \to |\Delta_\tau \pm \Delta\varepsilon|$. We will see that a smoother unitary transformation provides a less singular result.

A.2 Continuous unitary transformation (CUT)

It might be a surprise that the result (A.6) is not unique. But we emphasize that only the matrix elements on shell, i.e. without energy change, are defined independently from the chosen basis. All other matrix elements do depend on the chosen basis. Generally, a continuous change of basis is smoother and less singular than the one-step transformation, see also [57, 58].

The continuous change of the Hamiltonian is parameterized by $\ell \in [0, \infty)$ and $H_{\mathrm{F}}(\ell)$ is given by the differential equation

$$\partial_\ell H_{\mathrm{F}}(\ell) = [\eta(\ell), H_{\mathrm{F}}(\ell)]. \tag{A.7}$$

It is understood that $H_{\mathrm{F}}(\ell = 0)$ is given by the Hamiltonian H_{F} in (1a) while $H_{\mathrm{F}}(\ell = \infty)$ is given by H_{orb} in (3). The transformation (A.7) shall eliminate the terms in H_{F} which change the number of double occupancies, i.e. the kinetic part $H_{\mathrm{F}+} + H_{\mathrm{F}-}$.

Hence, we parameterize

$$H_{\mathrm{F}++}(\ell) = A_1(\ell) c^\dagger_{\alpha 1} c_{\beta 0} \hat{n}_{\alpha 0} + B_1(\ell) c^\dagger_{\beta 1} c_{\alpha 0} \hat{n}_{\beta 0}, \tag{A.8a}$$

$$H_{\mathrm{F}+-}(\ell) = A_0(\ell) c^\dagger_{\alpha 0} c_{\beta 1} \hat{n}_{\alpha 1} + B_0(\ell) c^\dagger_{\beta 0} c_{\alpha 1} \hat{n}_{\beta 1}, \tag{A.8b}$$

while $H_{\mathrm{F}0}$ remains constant in linear order in t; the operators $H_{\mathrm{F}--}(\ell) = (H_{\mathrm{F}++}(\ell))^\dagger$ and $H_{\mathrm{F}-+}(\ell) = (H_{\mathrm{F}+-}(\ell))^\dagger$ follow by Hermitean conjugation.

The crucial choice is the one for the infinitesimal generator $\eta(\ell)$. Our aim is to eliminate processes which create or annihilate excitations of the order of U'. Such an elimination can most easily be done by the Mielke–Knetter–Uhrig generator $\eta_{\mathrm{MKU}}(\ell)$ [59]–[61] which consists of the terms in the Hamiltonian increasing the number of excitations and of the negative terms in the Hamiltonian decreasing the number of excitations

$$\eta_{\mathrm{MKU}}(\ell) := H_{\mathrm{F}+}(\ell) - H_{\mathrm{F}-}(\ell). \tag{A.9}$$

For a general discussion see also [62]. With this choice one obtains in linear order in t

$$\partial_\ell H_{\mathrm{F}+}(\ell) = -[H_{\mathrm{F}+}(\ell), H_{\mathrm{F}0}], \tag{A.10}$$

which implies the differential equations

$$\partial_\ell A_1 = -(U' + \Delta_\alpha - \Delta\varepsilon) A_1, \tag{A.11a}$$

$$\partial_\ell A_0 = -(U' - \Delta_\beta - \Delta\varepsilon) A_0, \tag{A.11b}$$

$$\partial_\ell B_1 = -(U' + \Delta_\beta + \Delta\varepsilon) B_1, \tag{A.11c}$$

$$\partial_\ell B_0 = -(U' - \Delta_\alpha + \Delta\varepsilon) B_0. \tag{A.11d}$$

The solutions consist in decreasing exponential functions starting at t for $\ell = 0$ because we assume all the energy differences in the parentheses in equations (A.11a)–(A.11d) to be positive, i.e. U' dominates the other energies, see equations (4a) and (4b).

The orbital exchange is obtained by equating the second-order terms in t in (A.7) which implies

$$\partial_\ell J(\ell) b^\dagger_\alpha b^\dagger_\beta = 2[H_{\mathrm{F}++}(\ell), H_{\mathrm{F}-+}(\ell)]. \tag{A.12}$$

Since the right-hand side is given by the solutions of equations (A.11a)–(A.11d) an integration suffices to provide $J_{\mathrm{CUT}} = J(\ell = \infty)$

$$\begin{aligned} J_{\mathrm{CUT}} &= 2 \int_0^\infty (A_1(\ell) A_0(\ell) + B_1(\ell) B_0(\ell))\, \mathrm{d}\ell \\ &= \frac{t^2}{U' - \delta + ecE} + \frac{t^2}{U' + \delta - ecE} \\ &= \frac{2t^2 U'}{(U')^2 - (\delta - ecE)^2}, \end{aligned} \tag{A.13}$$

where we use the shorthand δ for the CF levels (see equation (6)), and E denotes the applied electric field. This is the result used in the main part of the paper, see equation (5).

Note that we retrieve the well-known result for the Heisenberg exchange of $2J = J_{\mathrm{Heisen}} = 4t^2/U'$ for $E = 0$ and $\delta = 0$, i.e. equivalent V sites.

Even more interesting is that $J_{\mathrm{CUT}} \neq J_{\mathrm{stan}}$. In particular, the individual excitation energies Δ_τ do not occur in J_{CUT} in (A.13) but only their difference (see equation (6)). Hence, a regime

exists with $\delta = 0$ and $\Delta_\tau \to U'$, where $J_{\rm stan}$ diverges while $J_{\rm CUT}$ remains unaffected. So the CUT result is less singular. Moreover, the expression for $J_{\rm CUT}$ is simpler than the one for $J_{\rm stan}$.

Tracing back from where the difference between the standard and the CUT results originates we have to compare equations (A.5) and (A.12). In the standard calculation (A.5), there is a striking asymmetry between the two operators which are commutated. Only one of them (η) carries information on the excitation energies. In the CUT calculation (A.12), both the commutated operators carry the dependence on the excitation energies in the same way by their dependence on ℓ. This implies also that a single commutation suffices because two commutators are equal while there are two different ones in (A.5).

For all the above reasons, we favor the CUT derivation. We stress, however, that in the regime relevant for YVO_3 the difference between $J_{\rm stan}$ and $J_{\rm CUT}$ is quantitatively of minor importance.

References

[1] Tokura Y and Nagaosa N 2000 *Science* **288** 462
[2] Khaliullin G 2005 *Prog. Theor. Phys. Suppl.* **160** 155
[3] Khomskii D I 2005 *Phys. Scr.* **72** CC8
[4] Lee S *et al* 2006 *Nat. Mater.* **5** 471
[5] Kugel K I and Khomskii D I 1973 *Sov. Phys.—JETP* **37** 725
[6] Jahn H A and Teller E 1937 *Proc. R. Soc.* A **161** 220
[7] Sugano S, Tanabe Y and Kamimura H 1970 *Multiplets of Transition-Metal Ions in Crystals* (New York: Academic)
[8] Ballhausen C F 1962 *Introduction to Ligand Field Theory* (New York: McGraw-Hill)
[9] Rückamp R *et al* 2005 *New J. Phys.* **7** 144
[10] Ishihara S and Maekawa S 2000 *Phys. Rev.* B **62** 2338
[11] Saitoh E, Okamoto S, Takahashi K T, Tobe K, Yamamoto K, Kimura T, Ishihara S, Maekawa S and Tokura Y 2001 *Nature* **410** 180
[12] Grüninger M, Rückamp R, Windt M and Freimuth A 2002 *Nature* **418** 39
[13] Ishihara S 2004 *Phys. Rev.* B **69** 075118
[14] Khaliullin G, Horsch P and Olés A M 2001 *Phys. Rev. Lett.* **86** 3879
[15] De Raychaudhury M, Pavarini E and Andersen O K 2007 *Phys. Rev. Lett.* **99** 126402
[16] Miyasaka S, Onoda S, Okimoto Y, Fujioka J, Iwama M, Nagaosa N and Tokura Y 2005 *Phys. Rev. Lett.* **94** 076405
[17] Miyasaka S, Fujioka J, Iwama M, Okimoto Y and Tokura Y 2006 *Phys. Rev.* B **73** 224436
[18] Sugai S and Hirota K 2006 *Phys. Rev.* B **73** 020409
[19] Ulrich C, Gössling A, Grüninger M, Guennou M, Roth H, Cwik M, Lorenz T, Khaliullin G and Keimer B 2006 *Phys. Rev. Lett.* **97** 157401
[20] Ulrich C, Ghiringhelli G, Piazzalunga A, Braicovich L, Brookes N B, Roth H, Lorenz T and Keimer B 2008 *Phys. Rev.* B **77** 113102
[21] Solovyev I V 2006 *Phys. Rev.* B **74** 054412
[22] Blake G R, Palstra T T M, Ren Y, Nugroho A A and Menovsky A A 2002 *Phys. Rev.* B **65** 174112
[23] Reehuis M, Ulrich C, Pattison P, Ouladdiaf B, Rheinstädter M C, Ohl M, Regnault L P, Miyasaka M, Tokura Y and Keimer B 2006 *Phys. Rev.* B **73** 094440
[24] Ren Y, Palstra T T M, Khomskii D I, Pellegrin E, Nugroho A A, Menovsky A A and Sawatzky G A 1998 *Nature* **396** 441
[25] Ren Y, Palstra T T M, Khomskii D I, Nugroho A A, Menovsky A A and Sawatzky G A 2000 *Phys. Rev.* B **62** 6577

[26] Miyasaka S, Okimoto Y, Iwama M and Tokura Y 2003 *Phys. Rev.* B **68** 100406
[27] Tsvetkov A A, Mena F P, van Loosdrecht P H M, van der Marel D, Ren Y, Nugroho A A, Menovsky A A, Elfimov I S and Sawatzky G A 2004 *Phys. Rev.* B **69** 075110
[28] Noguchi M, Nakazawa A, Oka S, Arima T, Wakabayashi Y, Nakao H and Murakami Y 2000 *Phys. Rev.* B **62** 9271
[29] Sawada H and Terakura K 1998 *Phys. Rev.* B **58** 6831
[30] Mizokawa T, Khomskii D I and Sawatzky G A 1999 *Phys. Rev.* B **60** 7309
[31] Fang Z and Nagaosa N 2004 *Phys. Rev. Lett.* **93** 176404
[32] Otsuka Y and Imada M 2006 *J. Phys. Soc. Japan* **75** 124707
[33] Bombik A, Lesniewska B and Oles A 1978 *Phys. Status Solidi* a **50** K17
[34] Ulrich C, Khaliullin G, Sirker J, Reehuis M, Ohl M, Miyasaka S, Tokura Y and Keimer B 2003 *Phys. Rev. Lett.* **91** 257202
[35] Horsch P, Khaliullin G and Oleś A M 2003 *Phys. Rev. Lett.* **91** 257203
[36] Miyashita S, Kawaguchi A, Kawakami N and Khaliullin G 2004 *Phys. Rev.* B **69** 104425
[37] Oleś A M, Horsch P and Khaliullin G 2007 *Phys. Rev.* B **75** 184434
[38] Blake G R, Nugroho A A, Palstra T T M and Gutmann M J 2008 *Phys. Rev.* B submitted
[39] Grüninger M *et al* 2002 *J. Phys. Chem. Solids* **63** 2167
[40] Miyasaka S, Okimoto Y and Tokura Y 2002 *J. Phys. Soc. Japan* **71** 2086
[41] Kasuya M, Tokura Y, Arima T, Eisaki H and Uchida S 1993 *Phys. Rev.* B **47** 6197
[42] Holstein T 1959 *Ann. Phys.* **8** 343
[43] Lorenzana J and Sawatzky G A 1995 *Phys. Rev. Lett.* **74** 1867
[44] Lorenzana J and Sawatzky G A 1995 *Phys. Rev.* B **52** 9576
[45] Gössling A, Schmitz R, Roth H, Haverkort M W, Lorenz T, Mydosh J A, Müller-Hartmann E and Grüninger M 2006 *Preprint* cond-mat/0608531
[46] Schmidt K P, Grüninger M and Uhrig G S 2007 *Phys. Rev.* B **76** 075108
[47] van den Brink J 2001 *Phys. Rev. Lett.* **87** 217202
[48] Rückamp R, Baier J, Kriener M, Haverkort M W, Lorenz T, Uhrig G S, Jongen L, Möller A, Meyer G and Grüninger M 2005 *Phys. Rev. Lett.* **95** 097203
[49] Ehrlich P and Seifert H-J 1959 *Z. Allg. Anorg. Chem.* **301** 282
[50] Fausti D *et al* 2007 *Phys. Rev.* B **75** 245114
[51] Mizokawa T and Fujimori A 1996 *Phys. Rev.* B **54** 5368
[52] Bussière G, Beaulac R, Cardinal-David B and Reber C 2001 *Coord. Chem. Rev.* **219–221** 509
[53] Ishii T, Ogasawara K and Adachi H 2002 *J. Chem. Phys.* **116** 471
[54] Tregenna-Piggott P L W, Spichiger D, Carver G, Frey B, Meier R, Weihe H, Cowan J A, McIntyre G J, Zahn G and Barra A-L 2004 *Inorg. Chem.* **43** 8049
[55] Grüninger M 1999 *PhD Thesis* University of Groningen, The Netherlands
[56] Oleś A M, Horsch P, Feiner L F and Khaliullin G 2006 *Phys. Rev. Lett.* **96** 147205
[57] Lenz P and Wegner F 1996 *Nucl. Phys.* B **482** 693
[58] Wegner F-J 1994 *Ann. Phys.* **3** 77
[59] Mielke A 1998 *Eur. Phys. J.* B **5** 605
[60] Uhrig G S and Normand B 1998 *Phys. Rev.* B **58** R14705
[61] Knetter C and Uhrig G S 2000 *Eur. Phys. J.* B **13** 209
[62] Knetter C, Schmidt K P and Uhrig G S 2003 *J. Phys. A: Math. Gen.* **36** 7889